The Astrophysical Journal, 605:493–502, 2004 April 10

THE EFFECTS OF STRATIFICATION ON OSCILLATING CORONAL LOOPS

César A. Mendoza-Briceño[1]
Centro de Astrofísica Teórica, Facultad de Ciencias, Universidad de los Andes, Apartado Postal 26, La Hechicera, Mérida 5251, Venezuela; cesar@ula.ve

Robert Erdélyi
Space & Atmosphere Research Center, Department of Applied Mathematics, University of Sheffield, Hicks Building, Hounsfield Road, Sheffield, S3 7RH, England, UK; robertus@sheffield.ac.uk

and

Leonardo Di G. Sigalotti
Centro de Física, Instituto Venezolano de Investigaciones Científicas, Apartado Postal 21827, Caracas 1020A, Venezuela; lsigalot@cassini.ivic.ve
Received 2003 August 28; accepted 2003 December 19

ABSTRACT

Recent observations by the *Solar and Heliospheric Observatory* (*SOHO*) and the *Transition Region and Coronal Explorer* (*TRACE*) have confirmed previous theoretical predictions that coronal loops may oscillate. These oscillations and their damping are of fundamental importance, because they can provide diagnostics of the coronal plasma. In the present paper, we perform numerical hydrodynamic calculations of a one-dimensional loop model to investigate the effects of stratification on damping of longitudinal waves in the hot coronal loops observed by the Solar Ultraviolet Measurements of Emitted Radiation (SUMER) on board the *SOHO* satellite. In particular, we study the dissipation by thermal conduction and by compressive viscosity of standing slow magnetosonic disturbances in loops of semicircular shape. For the parameter regime that characterizes the SUMER hot loops, we find that stratification results in a ~10%–20% reduction of the wave-damping time compared to the nonstratified loop models because of increased dissipation by compressive viscosity due to gravity. We show that temperature oscillations are more strongly dissipated by thermal conduction, while density and velocity waves are mostly damped by compressive viscosity. However, the decay time of the oscillations is always governed by the thermal conduction timescale. The scalings of the decay time with wave period, temperature, and loop length all point toward higher dissipation rates in the stratified, hotter loops because of the increased effects of thermal conduction and compressive viscosity.

Subject headings: hydrodynamics — methods: numerical — Sun: activity — Sun: atmosphere — Sun: corona — waves

1. INTRODUCTION

Recent EUV observations of low-β regions in the upper solar atmosphere (i.e., the transition region and corona) by the space missions *Solar and Heliospheric Observatory* (*SOHO*) and *Transition Region and Coronal Explorer* (*TRACE*) (e.g., Domingo, Fleck, & Poland 1995; Handy et al. 1999; Aschwanden, Schrijver, & Alexander 2001) have revealed the presence of magnetic loop structures, often configured in the form of arches or spikes, with a wealth of sizes and timescales. Significant dynamic activity has also been discovered in these loops; their physical structure is characterized by transient brightenings and sustained flow of plasma material along the arched magnetic field lines, which describe the shape and geometry of the loops. Since the dynamics of the plasma in the solar transition region and corona is dominated by magnetic fields, the apparent turbulent state in which physical processes at different scales are related in the upper solar atmosphere may well be of magnetohydrodynamic (MHD) origin.

A major question in solar physics concerns the heating of the coronal plasma. Although considerable theoretical and observational effort has gone into trying to answer it, the problem still remains. Out of the several mechanisms that have been proposed for explaining the heating of coronal loops, MHD turbulence has recently been suggested as a highly viable one (Chae, Poland, & Aschwanden 2002). In this picture, perturbations that are produced by photospheric shuffling motions near the loop footpoints propagate along the loop length, making the magnetic field and plasma velocity fluctuate. Turbulent motion ultimately arises as the amplitudes of these oscillations grow and develop nonlinearly. The magnetic and kinetic energy carried by the fluctuations are then conveyed from the largest to the smallest eddies until they are converted into heat by ohmic and viscous dissipation. On the other hand, the damping of coronal loop oscillations has also recently received great interest, since it may be associated with dissipating wave motions, which could represent a possible source of coronal heating. Such waves may be used as true diagnostic tools to infer the physical parameters of the coronal plasma (Roberts, Edwin, & Benz 1984; Nakariakov & Ofman 2001).

Observations using the white-light channel of the Ultraviolet Coronagraph Spectrometer (UVCS) on *SOHO* that reveal the presence of periodic density fluctuations in coronal plumes high above the solar limb have been reported by Ofman et al. (1997). They interpreted these variations as being due to compressional waves propagating in the polar coronal holes. In

[1] Also at: Space and Atmosphere Research Center, Department of Applied Mathematics, University of Sheffield, Hicks Building, Hounsfield Road, Sheffield S3 7RH, England, UK; c.mendoza@sheffield.ac.uk.

addition, the presence of wave trains traveling through polar plumes with periods of 10–15 minutes has also been detected from *SOHO* EUV Imaging Telescope (EIT) data by DeForest & Gurman (1998), who identified such perturbations as sonic or slow-mode magnetosonic waves. Similarly, using EIT and *TRACE*, respectively, Berghmans & Clette (1999) and De Moortel, Ireland, & Walsh (2000) reported evidence for highly resolved longitudinal waves in coronal loops. Transverse-mode oscillations excited by flares in coronal loops were also observed in EUV radiation by *TRACE* (see Aschwanden et al. 1999; Nakariakov et al. 1999). More recently, Schrijver, Aschwanden, & Title (2002) presented an extensive overview of *TRACE* observations of transverse coronal loop oscillations, while Aschwanden et al. (2002) provided a detailed discussion of the periods, amplitudes, and other parameters obtained from these observations. These studies suggest that transverse loop oscillations may be the result of the evolution of impulsively generated MHD waves and that their rapid decay could be related to photospheric leakage of wave energy at the loop footpoints. Recently, the Solar Ultraviolet Measurements of Emitted Radiation (SUMER) spectrometer on board the *SOHO* satellite detected large Doppler-shift velocities with strong oscillatory damping in hot ($T > 6$ MK) coronal loops (Kliem et al. 2002; Wang et al. 2002a, 2002b, 2002c). These oscillations were interpreted as signatures of standing, slow or kink magnetosonic waves excited impulsively in the loops (Ofman & Wang 2002). Moreover, Sakurai et al. (2002) presented a time sequence over 80 minutes of coronal green-line spectra obtained with a ground-based coronagraph at the Norikura Solar Observatory. They also detected Doppler-shift oscillations and interpreted them as being due to propagating, rather than standing, slow-mode MHD waves. Strong observational evidence for standing slow-mode waves in hot postflare loops has only recently been recorded by Wang et al. (2003b), and an extensive survey of Doppler-shift oscillations in hot coronal loops obtained with SUMER by Wang et al. (2003a) has revealed that they have periods from about 7.1 to 31.1 minutes and decay times in the range of 5.7–36.8 minutes. It is believed that slow-mode waves are excited by disturbances having large turbulent velocities associated with the ejection of hot plasma from one footpoint of a coronal loop. This may explain the observed concurrence of initial strong Doppler shifts and line broadenings (Wang et al. 2003a). It is also possible that line broadening may be due to the overlapping of several loops in the line of sight, all of them oscillating with different phases. However, in this case we would expect the line broadening to be nearly constant or to exhibit a rather chaotic behavior in contrast with its periodic character, as inferred by Wang et al. (2002c, 2003a).

Compared to the hot loops, the oscillations detected in cool coronal loops by *TRACE* (see, e.g., Aschwanden et al. 2002) are characterized by much shorter periods and smaller amplitudes, implying that they may correspond to transverse (kink-mode) waves propagating with a comparatively higher phase speed than the Doppler-shift oscillations in the SUMER hot loops. The identification of different modes of oscillation in hot and cool loops is important, because different dissipation mechanisms may act, depending on the wave mode. For instance, slow magnetosonic waves are more easily dissipated by thermal conduction or compressive viscosity, while fast transverse waves dissipate by resistivity or shear viscosity. In particular, Ofman & Wang (2002) found that thermal conduction is the primary dissipation mechanism of slow waves in hot coronal loops. A theoretical description of the damping of slow MHD waves has recently been given by De Moortel & Hood (2003). They also concluded, from a linear analysis of the damping of slow-mode waves in nonstratified, isothermal plasma loop models, that thermal conduction is the dominant dissipation mechanism of slow waves in coronal loops and that the contribution of compressive viscosity is less significant. In contrast with these previous findings, here we show that in hot ($T > 6.0$ MK) loops, disturbances in the density and velocity are more easily dissipated by compressive viscosity, while temperature oscillations are more strongly damped by thermal conduction. The occurrence of larger velocity gradients under gravity enhances the dissipative effects of compressive viscosity in stratified loops. However, the concurrence of both mechanisms is necessary to reproduce the observed periods and decay times.

Numerical simulations of the damping of slow MHD waves by viscosity were performed by Ofman, Nakariakov, & Sehgal (2000) in one- and two-space dimensions. The effects of thermal conduction, viscosity, and gravity on slow-wave damping in a one-dimensional coronal loop model were considered by Nakariakov et al. (2000) in the limit of small dissipation and excluding self-consistent heating. The damping of slow magnetosonic waves by thermal conduction in the cool loops observed with *TRACE* was studied by De Moortel et al. (2002). Finally, Ofman & Wang (2002) performed one-dimensional calculations of the damping of moderately nonlinear slow MHD waves in a hot coronal loop model with typically observed solar parameters, including large dissipation by thermal conduction, viscosity, and self-consistent heating. Here, by "large dissipation" we mean that the damping timescale is comparable to the oscillation period. In the present work, we extend the model calculations of Ofman & Wang (2002) to include the effects of stratification on the damping of standing slow magnetosonic oscillations in hot coronal loops. In § 2 we present the basic equations to be solved, along with a brief description of the loop model and the numerical methods employed. The results of the calculations are described in § 3, while § 4 contains the conclusions.

2. BASIC EQUATIONS AND LOOP MODELS

The thermodynamical evolution of the solar coronal plasma is constrained by the geometry of the magnetic field such that both the mass flow and heat conduction in coronal loops occurs primarily along the field lines. In addition, for most loops the structure of the magnetic field does not change appreciably during the plasma evolution, because the Alfvén travel time is usually much shorter than the evolution time. Hence, to a good approximation we may assume a one-dimensional coronal loop model, in which all quantities vary along the field lines, and solve the conservative form of the hydrodynamic equations in a Cartesian frame of reference. Including the effects of solar gravity, thermal conduction, and viscosity, these equations are

$$\frac{\partial \rho}{\partial t} + \frac{\partial (\rho v)}{\partial s} = 0, \tag{1}$$

$$\frac{\partial (\rho v)}{\partial t} + \frac{\partial (\rho v^2)}{\partial s} = -\frac{\partial p}{\partial s} + \rho g(s) + F_\eta, \tag{2}$$

$$\frac{\partial (\rho T)}{\partial t} + \frac{\partial (\rho v T)}{\partial s} = -\frac{\mu(\gamma - 1)}{R_g}\left[p\frac{\partial v}{\partial s} - \frac{\partial}{\partial s}\left(\kappa \frac{\partial T}{\partial s}\right) - E_\eta\right], \tag{3}$$

where t is time, s denotes the position along a loop of constant cross-sectional area, ρ is the (mass) density, v is the fluid velocity, T is the plasma temperature, p is the gas pressure, $g(s)$ is the component of solar gravity along the field line, μ is the mean molecular weight, R_g is the gas constant, $\gamma(=5/3)$ is the ratio of specific heats, and $\kappa = 1.0\times10^{-6}T^{5/2}$ ergs cm^{-1} s^{-1} K^{-1} is the coefficient of thermal conductivity parallel to the magnetic field (Braginskii 1965). In equations (2) and (3), F_η and E_η denote the viscous force and the viscous heating terms, given by

$$F_\eta = \frac{4}{3}\frac{\partial}{\partial s}\left(\eta\frac{\partial v}{\partial s}\right), \tag{4}$$

$$E_\eta = \frac{4}{3}\eta\left(\frac{\partial v}{\partial s}\right)^2, \tag{5}$$

respectively, where η is the coefficient of compressive viscosity defined (Braginskii 1965) as

$$\eta = \frac{0.72\left(m_p k_B^5\right)^{1/2}}{\pi^{1/2}e^4\ln\lambda}T^{5/2} = \eta_0 T^{5/2}. \tag{6}$$

Here, m_p is the proton mass, k_B is the Boltzmann constant, e is the electron charge, and $\ln\lambda \approx 23$ is the Coulomb logarithm. Note that relation (6) is the same used by Ofman & Wang (2002). The gravity term on the right-hand side of equation (2) is assumed to depend only on position along the loop and is given by

$$g(s) = -g_\odot\cos\left(\frac{\pi s}{L}\right), \tag{7}$$

where $g_\odot \approx 2.74\times10^4$ cm s^{-2} is the solar surface gravity and L is the total length of the loop. As shown in Figure 1, equation (7) specifies the component of gravity along a magnetic field line of semicircular shape only. In the present model, the entire semicircle is represented by the calculations. Equations (1)–(3) are solved in closed form by assuming the pressure relation $p = R_g\rho T/\mu$.

In common with Ofman & Wang (2002), we neglect the effects of radiative losses on the right-hand side of equation (3) under the assumption that they occur on a timescale longer than the observed wave-damping time. In the stratified models, the initial density profile is calculated from the condition of hydrostatic equilibrium, which is obtained from equation (2) by setting the velocity to zero, while in the nonstratified cases, the density profile is assumed to be uniform. In both cases, the initial temperature is assumed to be uniform along the loop, and the initial velocity is given an oscillatory dependence on position of the form $v = v_0\sin(2\pi sk/L)$, where v_0 is the amplitude of the wave at $t = 0$ and k is the wavenumber taken to be unity. Appropriate boundary conditions at the footpoints are specified by setting the velocity there to zero and enforcing continuity conditions (i.e., zeroth-order extrapolation) for the density and temperature. Test calculations using a slightly different treatment of the boundary conditions, in which both the density and temperature are evolved hydrodynamically at the footpoints, yielded essentially the same results.

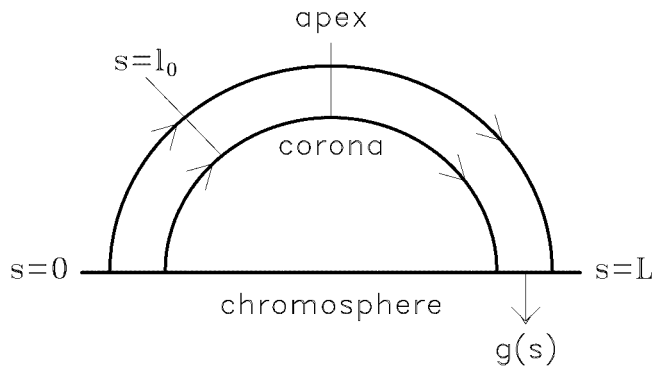

FIG. 1.—Geometry of the one-dimensional loop model. Here L is the total length of the loop, and s is the position on the loop increasing in a clockwise sense. The distance l_0 from the left footpoint marks the location on the loop where the time evolution of the hydrodynamic quantities is displayed.

Equations (1)–(3) are solved numerically using a one-dimensional, finite-difference (FD) hydrodynamics code based on a temporally and spatially second-order accurate Lagrangian remap technique (Sigalotti & Mendoza-Briceño 2003). The code employs a nonstaggered linear Cartesian mesh in which all variables are assigned to the zone centers s_i. The equations are first rewritten in Lagrangian form, and their discretized representations are solved in a predictor-corrector fashion to update the density, velocity, and temperature. Both the predictor and corrector steps rely on a multistep solution procedure in which the source contributions on the right-hand sides of equations (2) and (3) are evaluated separately. After completion of the Lagrangian step, the solution is mapped back onto an Eulerian grid, which can be either fixed or moving, by assuming piecewise-linear representations of the fundamental variables to preserve the second-order accuracy of the Lagrangian solver. The discretized remap equations for the density, momentum, and internal energy are constructed from the laws of mass, momentum, and energy conservation, respectively. A full description of the multistep Lagrangian procedure and Eulerian remap, including a detailed account of the gravity, thermal conduction, and cooling and heating solvers, is found in Sigalotti & Mendoza-Briceño (2003). For the sake of completeness here we briefly describe how the viscous force F_η and heating E_η are incorporated into the code. These effects are quantified by solving the "substep" integral equations

$$\frac{d}{dt}\int_s \rho v\,ds = \frac{4}{3}\int_s \frac{\partial}{\partial s}\left(\eta\frac{\partial v}{\partial s}\right)ds \tag{8}$$

and

$$\frac{d}{dt}\int_s \rho T\,ds = \frac{4}{3}\frac{\mu(\gamma-1)}{R_g}\int_s \eta\left(\frac{\partial v}{\partial s}\right)^2 ds, \tag{9}$$

where the spatial integration is over the size Δs of a given grid zone.

In particular, equation (8) is solved implicitly for the velocity, after partial updates of the Lagrangian positions s_i and velocities v_i due to gravity and pressure forces are obtained. The implicit solution is accomplished by direct integration of equation (8) into the FD form

$$\frac{v_i^{n+1}-v_i^n}{\Delta t} = \frac{2}{3}\left(\frac{\eta_i+\eta_{i+1}}{\rho_i\Delta s_i}\right)\left(\frac{v_{i+1}-v_i}{s_{i+1}-s_i}\right) - \frac{2}{3}\left(\frac{\eta_i+\eta_{i-1}}{\rho_i\Delta s_i}\right)\left(\frac{v_i-v_{i-1}}{s_i-s_{i-1}}\right), \tag{10}$$

where the superscripts denote the time level (i.e., $t^{n+1} = t^n + \Delta t$) and the subscripts are used to label zone-centered quantities. Here the superscript n on the left-hand side of equation (10) refers to quantities at the end of the fluid-acceleration substep due to gravity and pressure forces, while the terms on the right-hand side are meant to be time-centered, that is, evaluated at the intermediate time $t^{n+1/2} = (t^n + t^{n+1})/2$. Substitution of the time-centered values in equation (10) leads to a set of linear algebraic equations of the form

$$-\alpha_i^{n+1/2} v_{i+1}^{n+1} + \beta_i^{n+1/2} v_i^{n+1} - \gamma_i^{n+1/2} v_{i-1}^{n+1} = \delta_i^{n+1/2}, \quad (11)$$

which can be solved for the updated velocities by means of a tridiagonal matrix algorithm. Note that these final updates contain the contribution effects of all forces entering the right-hand side of equation (2). Final new Lagrangian positions then follow from

$$s_i^{n+1} = s_i^n + \frac{1}{2}\Delta t\left(v_i^n + v_i^{n+1}\right), \quad (12)$$

where the superscript n now refers to old quantities at the beginning of the Lagrangian step.

An implicit solver is also enforced for equation (9), which is integrated only after the thermal conduction substep is completed. A rapidly convergent fifth-order Newton-Raphson iteration scheme is implemented to solve it implicitly. The updated temperatures from this substep are then used to perform compressional work on the gas, after which final updates for the temperature and specific internal energy follow. The calculations in this paper were carried out using 257 initially uniformly spaced zones along the semicircular loop. Tests with lower (101 zones) and higher (up to 501 zones) initial resolution converged essentially to the same results. Since the Eulerian mesh is allowed to closely follow the Lagrangian motion, the present method is adaptive in nature.

3. RESULTS AND DISCUSSION

The aim of the present model calculations is to quantify the effects of stratification on damping of the Doppler-shift oscillations observed by SUMER in hot ($T > 6$ MK) coronal loops. To do so, we start from the same loop parameters used by Ofman & Wang (2002), who performed similar calculations of the damping of slow MHD waves in hot loops, by neglecting the effects of solar gravity. In particular, we choose a one-dimensional loop configuration of semicircular shape, constant cross-sectional area, and total length $L = 400$ Mm ($\approx 0.575\ R_\odot$), with an initial uniform temperature ($T = 6.3$ or 8.0 MK) distribution. For the nonstratified models, an initial uniform density ($= 5.0 \times 10^8$ cm^{-3}) distribution is used. As outlined by Ofman & Wang (2002), these initial parameters are motivated by SUMER and *Yohkoh* Soft X-Ray Telescope (SXT) observations of hot loops in the upper solar atmosphere. With this choice, the coefficient of compressive viscosity given by equation (6) takes values of $\eta \approx 9.58$ g cm^{-1} s^{-1} for $T = 6.3$ MK and ≈ 17.40 g cm^{-1} s^{-1} for $T = 8.0$ MK, while the coefficient of thermal conductivity is $\kappa \approx 9.96 \times 10^{10}$ ergs cm^{-1} s^{-1} K^{-1} for $T = 6.3$ MK and $\approx 1.81 \times 10^{11}$ ergs cm^{-1} s^{-1} K^{-1} for $T = 8.0$ MK. Note that these latter values are slightly higher than those quoted by Ofman & Wang (2002). Thus, in the absence of gravity, our models differ from theirs, only in slightly enhancing the effects of thermal conduction.

3.1. *Damping of Standing Slow-Mode Waves*

Loop oscillations in the form of standing slow magnetosonic waves are introduced by allowing the initial velocity to oscillate with position along the loop, with a prescribed constant amplitude v_0. In order to check the ability of the code to reproduce the results obtained by Ofman & Wang (2002), we consider initial wave-velocity amplitudes of 20 and 87 km s^{-1} in a nonstratified loop model and then compare the results for the same parameters to those obtained in the stratified case. In Figure 2, we display the resulting time evolution of the wave velocity (Fig. 2*a*), density (Fig. 2*b*), and temperature (Fig. 2*c*) at a fixed distance $l_0 = 0.35L$ ($\approx 0.20\ R_\odot$) from the left footpoint at $s = 0$ (see Fig. 1) for the particular case in which $T = 8.0$ MK and $v_0 = 87$ km s^{-1}. The solid line in Figures 2*a*–2*c* depicts the wave evolution in the stratified loop (i.e., with gravity included), while the dashed line shows the same evolution with no stratification (i.e., with no gravity). The fits of the exponential decay of the amplitude $v_0 \exp(-t/t_d)$, where t_d is the dissipation time, are also shown in Figure 2*a* with the dot-dashed line (no stratification) and triple-dot–dashed line (stratification) curves. In the stratified case, the wave velocity has a period of ≈ 1163 s (≈ 19.4 minutes) and a decay time of about 1231 s (≈ 20.5 minutes). For comparison, the wave in the nonstratified loop has a slightly shorter period (≈ 1153 s [≈ 19.2 minutes]) and a longer decay time (≈ 1396 s [≈ 23.3 minutes]). In both cases, the wave velocity almost completely dissipates after about 4000 s (≈ 66.7 minutes), with the wave in the stratified loop reaching smaller amplitudes ($v \approx 2.72$ km s^{-1}, by 3601 s) faster than in the nonstratified ($v \approx 4.10$ km s^{-1}, by 3553 s) case.

The above results point to a reduction of the decay time by about 12% when gravity is included. With our choice of standard hot coronal plasma parameters and the loop-aligned form of gravity given by equation (7), the pressure scale height

$$\lambda_p = -\left(\frac{1}{p}\frac{dp}{ds}\right)^{-1} = -\frac{p}{\rho g(s)} \quad (13)$$

is found to vary from $\approx 0.80L$ ($T = 6.3$ MK) and $\approx 1.01L$ ($T = 8.0$ MK) at the footpoint ($s = 0$), to infinity at the summit ($s = L/2$), where $g(s)$ exactly vanishes. At the observation point ($s = l_0 = 0.35L$), the pressure scale height becomes approximately twice the loop length ($L = 400$ Mm) with $\lambda_p \approx 1.75L$ for $T = 6.3$ MK and $\approx 2.23L$ for $T = 8.0$ MK. These values clearly indicate that gravity contributes more to enhancing wave dissipation near the footpoint, where $\lambda_p \lesssim L$, than toward the summit, where $\lambda_p \to \infty$. The presence of gravity causes the plasma to be more strongly accelerated away from the summit, producing larger velocity gradients along the loop and hence increased viscous dissipation (see § 3.2).

The temporal evolution of the density and temperature perturbations calculated as $\delta\chi/\chi = [\chi(s = l_0, t) - \chi_i]/\chi_i$, where χ_i denotes the initial ($t = 0$) value of either ρ or T at $s = l_0$, are shown in Figures 2*b* and 2*c*, respectively. As in Ofman & Wang (2002), we see that the temperature oscillates with amplitudes that are much smaller than those of the density, with both waves exhibiting about a quarter-period phase difference compared to the velocity. This latter result supports the observational evidence that for standing slow-mode waves in hot loops, the intensity fluctuations lag the Doppler shifts by a quarter period (Wang et al. 2003a). From Figure 2 we also see that all three waves dissipate on essentially the same timescale, independently of whether gravity is included or

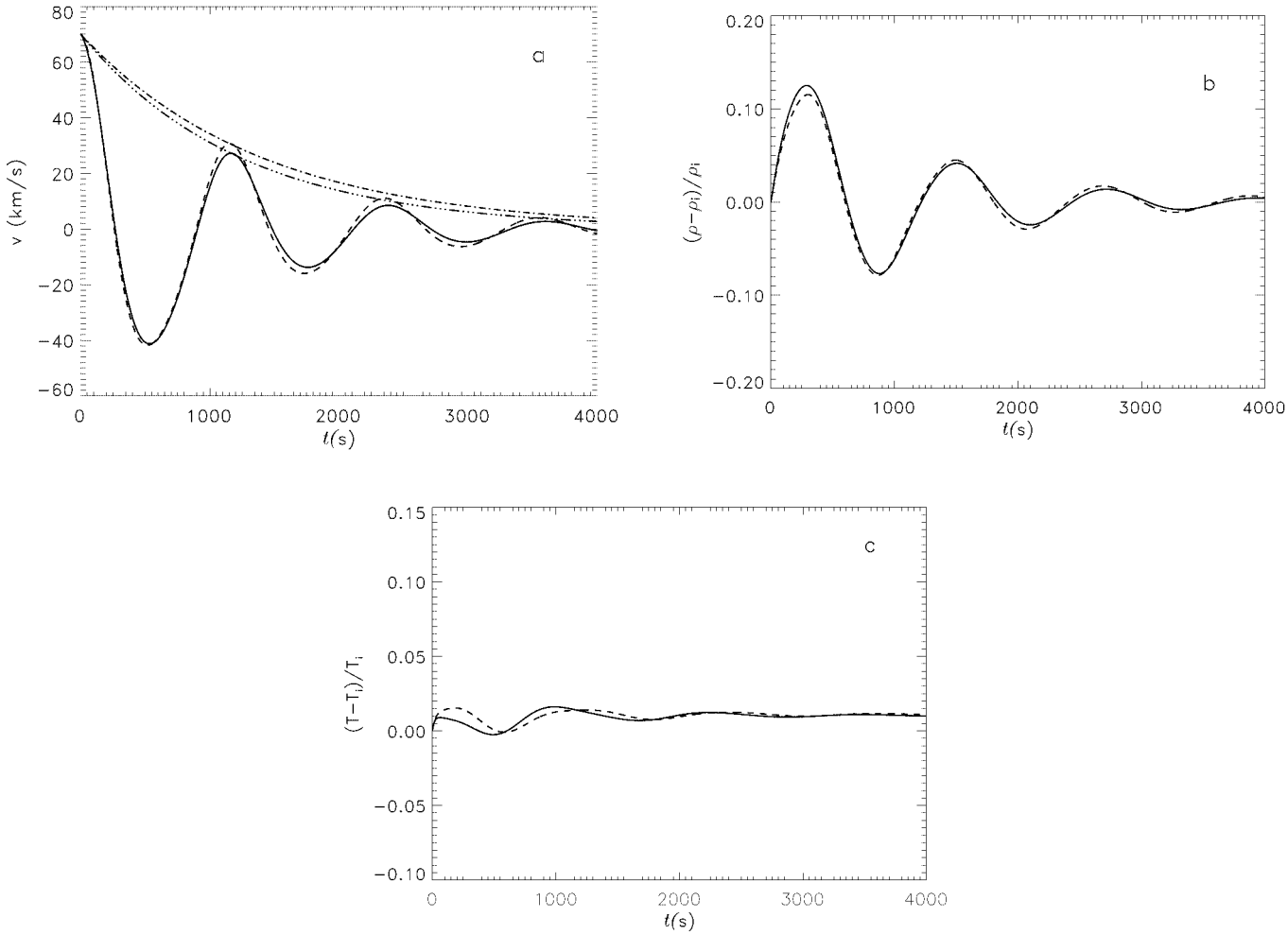

FIG. 2.—Time evolution of the (*a*) wave velocity, (*b*) density, and (*c*) temperature at $s = l_0 = 0.35L$ for a loop model with $T = 8.0$ MK and $L = 400$ Mm. In all panels, the time evolution of the waves in a stratified loop (*solid line*) is compared with that in a nonstratified medium (*dashed line*) for an initial wave-velocity amplitude of 84 km s^{-1}. The fits of the exponential wave damping are shown in (*a*) with the dot-dashed and triple-dot–dashed curves for the nonstratified and stratified loop, respectively.

excluded. In the cooler ($T = 6.3$ MK) loops, both the period and the decay time of the slow waves are longer compared to those in the hotter ($T = 8.0$ MK) models. In addition, the predicted ratio of decay time to period is ~1.6 for both the stratified and nonstratified $T = 6.3$ MK loops, whereas $t_d/P \sim 1.1$ and 1.2 for the stratified and nonstratified $T = 8.0$ MK models, respectively. These ratios are within the range of values (0.3–2.1) inferred observationally by Wang et al. (2003a) on the basis of data of 54 Doppler-shift oscillations associated with 27 flux-enhancement events of hot plasma. As we see below, the result that the decay time becomes shorter at higher temperatures is consistent with both thermal conduction and compressive viscosity being the dominant mechanisms for the damping of coronal loop oscillations.

In particular, in the stratified case when $T = 6.3$ MK, the wave velocity has a period of ≈1306 s (≈21.8 minutes) and a decay time of ≈2062 s (≈34.4 minutes) for an initial wave amplitude of 87 km s^{-1}. These results compare favorably with the period (~16.8 minutes) and decay time (~36.8 minutes) measured by Wang et al. (2003b) for one Doppler-shift oscillation produced by an M-class flare and recorded in an Fe XIX line by SUMER, in a loop with $T = 6.3$ MK and length $L = 191$ Mm. By ~4016 s, the velocity at $s = l_0$ is ≈5.75 km s^{-1}, corresponding to approximately 8% of its value at $t = 0$. As expected, this amplitude is higher than the 4% value found for the $T = 8.0$ MK loop model at a comparable evolution time. While the above predicted periods and decay times are toward the intermediate ($T = 8$ MK) and upper ($T = 6.3$ MK) parts of the range of values observed by *SOHO* in hot coronal loops, we find that the main effect of stratification is to reduce the dissipation time of slow-mode waves by ~10%–20% compared to the nonstratified models. With the same initial parameters and spatial resolution, the results displayed in Figure 2 for the nonstratified loop case are qualitatively similar to those obtained by Ofman & Wang (2002, Fig. 2). The small quantitative differences in the values of the wave period and decay time as well as the amplitude of the temperature oscillations (Fig. 2*c*) can be attributed to differences in the numerical methods employed.

The scaling of the decay time with wave period for all of the previous models is shown in Figure 3. The linear scaling is well reproduced with $t_d \approx 0.48P^{1.171}$ ($T = 6.3$ MK; *open circles*) and $t_d \approx 0.66P^{1.086}$ ($T = 8.0$ MK; *filled circles*) for the nonstratified loops. Stratification is found to slightly lower the power of the scaling to $t_d \approx 0.47P^{1.168}$ for $T = 6.3$ MK (*plus signs*) and $\approx 0.63P^{1.073}$ for $T = 8.0$ MK (*asterisks*). These theoretical predictions fall well within the observational band of scalings, $t_d = 0.68^{+0.46}_{-0.17}P^{1.06\pm0.18}$, derived by Wang

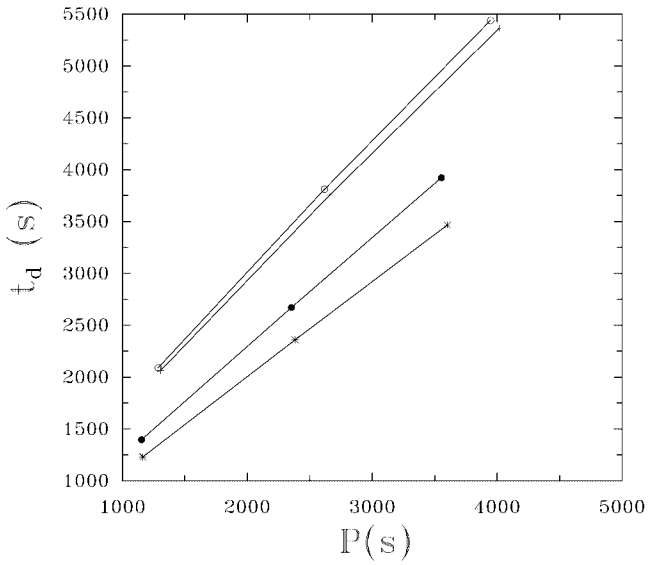

FIG. 3.—Predicted scaling of the decay time with wave period for the stratified and nonstratified loop model calculations with $T = 6.3$ and 8.0 MK. The data set plotted corresponds to models with an initial wave-velocity amplitude of $v_0 = 87$ km s^{-1}. The open circles give the scaling for $T = 6.3$ MK with no stratification, the plus signs for $T = 6.3$ MK with stratification, the filled circles for $T = 8.0$ MK with no stratification, and the asterisks for $T = 8.0$ MK with stratification.

et al. (2003a) from a sample of 49 out of 54 Doppler-shift oscillations in hot ($T > 6.0$ MK) loops observed by SUMER. Note that the power of the scalings for the $T = 6.3$ and 8.0 MK loop models points toward higher dissipation rates for the same wave period in the hotter ($T = 8.0$ MK) cases, consistent with the increased efficiency of thermal conduction and compressive viscosity at high temperatures. In addition, for the same temperature and wave period, the dissipation rates are higher in the stratified loops compared to the nonstratified ones. As expected, this latter feature becomes more evident for the hotter loops, because both the increased temperature and the larger velocity gradients induced by gravity lead to increased viscous dissipation (see § 3.2). For comparison, Ofman & Wang (2002) obtained powers of the scaling of 1.17 for $T = 6.3$ MK and 1.01 for $T = 8.0$ MK in loop models with no stratification.

3.2. *Effects of Thermal Conduction and Compressive Viscosity*

In order to evaluate the dissipative effects of thermal conduction and viscosity on wave damping, we have performed separate runs by setting either $\kappa = 0$ or $\eta = 0$ in equations (1)–(3) for both the $T = 6.3$ and 8.0 MK cases when $v_0 = 87$ km s^{-1}. For simplicity, we first center the discussion on the results for the nonstratified models and then compare the results with those obtained for the stratified loops. The importance of viscosity and thermal conduction can be quantified in terms of dimensionless parameters (De Moortel & Hood 2003), namely,

$$\epsilon = \frac{1}{\mathrm{Re}} = \frac{\eta}{\rho L c_s}, \tag{14}$$

$$d = \frac{(\gamma - 1)\kappa \rho T c_s}{\gamma^2 p^2 L} = \frac{1}{\gamma}\frac{\tau_s}{\tau_{\mathrm{cond}}}, \tag{15}$$

respectively, where Re is the Reynolds number, $c_s^2 = \gamma p/\rho$ is the adiabatic sound speed, $\tau_s = L/c_s$ is the sound travel time, and $\tau_{\mathrm{cond}} = L^2 p/(\gamma - 1)\kappa T$ is the thermal conduction timescale. For reference, the viscous timescale is $\tau_{\mathrm{visc}} = 3L^2\rho/4\eta$. For the nonstratified models, where the density and temperature are initially uniform, we obtain $\epsilon \approx 0.0075$ and $d \approx 0.23$ for $T = 6.3$ MK, and $\epsilon \approx 0.012$ and $d \approx 0.36$ for $T = 8.0$ MK. These values closely correspond to those quoted by De Moortel & Hood (2003) in their linear analysis of the damping of standing waves observed by SUMER. With this choice of parameters, $\tau_{\mathrm{visc}} \approx 37.5\tau_{\mathrm{cond}}$, where $\tau_{\mathrm{cond}} \approx 46.5$ minutes for $T = 6.3$ MK and $\tau_{\mathrm{cond}} \approx 25.6$ minutes for $T = 8.0$ MK. For comparison, $\tau_s \approx 17.5$ minutes (for $T = 6.3$ MK) and $\tau_s \approx 15.5$ minutes (for $T = 8.0$ MK). The conductive times are comparable to the decay times obtained for the models of § 3.1 when both thermal conduction and viscosity are included. Evidently, the decay time of the amplitude of slow-mode oscillations in hot coronal loops is determined by the conduction timescale.

We may gain some insight on the dissipational effects of thermal conduction and compressive viscosity using linear analysis. This is justified for our standing-wave initial conditions ($v_0 = 20$ and 87 km s^{-1}), because the resulting wave amplitudes ($\lesssim 0.1L$) are always much less than the pressure scale height ($\gtrsim L$), implying that nonlinear effects should be rather small. In the absence of gravity, linearization of equations (1)–(3) leads to the same forms given by equations (9)–(12) of De Moortel & Hood (2003) for the velocity (v), density (ρ), temperature (T), and pressure (p) perturbations. In particular, when $d = 0$ (i.e., no thermal conduction), these linearized equations can be combined to yield the wave-velocity equation

$$\frac{\partial^2 v}{\partial t^2} = \frac{\partial^2 v}{\partial s^2} + \frac{4}{3}\epsilon \frac{\partial}{\partial t}\left(\frac{\partial^2 v}{\partial s^2}\right), \tag{16}$$

coupled with the forms

$$\frac{\partial \rho}{\partial t} = -\frac{\partial v}{\partial s}, \tag{17}$$

$$\frac{\partial T}{\partial t} = -(\gamma - 1)\frac{\partial v}{\partial s} \tag{18}$$

for the temporal evolution of the density and temperature fluctuations. Note that viscous heating contributes with second-order terms, and therefore it does not appear in equation (18). From the above equations, we can see that the velocity oscillations are always dissipated by compressive viscosity, while the density and temperature oscillations damp out mainly by hydrodynamic coupling via the velocity gradients. In order to provide direct comparison with the models of Figure 2, we show in Figure 4 the resulting time evolution of the wave velocity (Fig. 4*a*), density (Fig. 4*b*), and temperature (Fig. 4*c*) at $s = l_0 = 0.35L$ when $\kappa = 0$, for the specific case in which $T = 8.0$ MK and $v_0 = 87$ km s^{-1}. The solid line shows the wave evolution in the stratified loop, and the dashed line shows the same evolution in the absence of gravity (no stratification). Compared to the $T = 6.3$ MK case, the results show a much stronger damping for all three waves in the hotter loop (see Fig. 4), in accordance with the fact that viscous dissipation is enhanced at higher temperatures (i.e., $\epsilon \propto T^{5/2}$). As a consequence, the presence of higher harmonics due to nonlinearity and viscous heating is also much less evident in the hotter loop than in the cooler one. Increased temperature also results

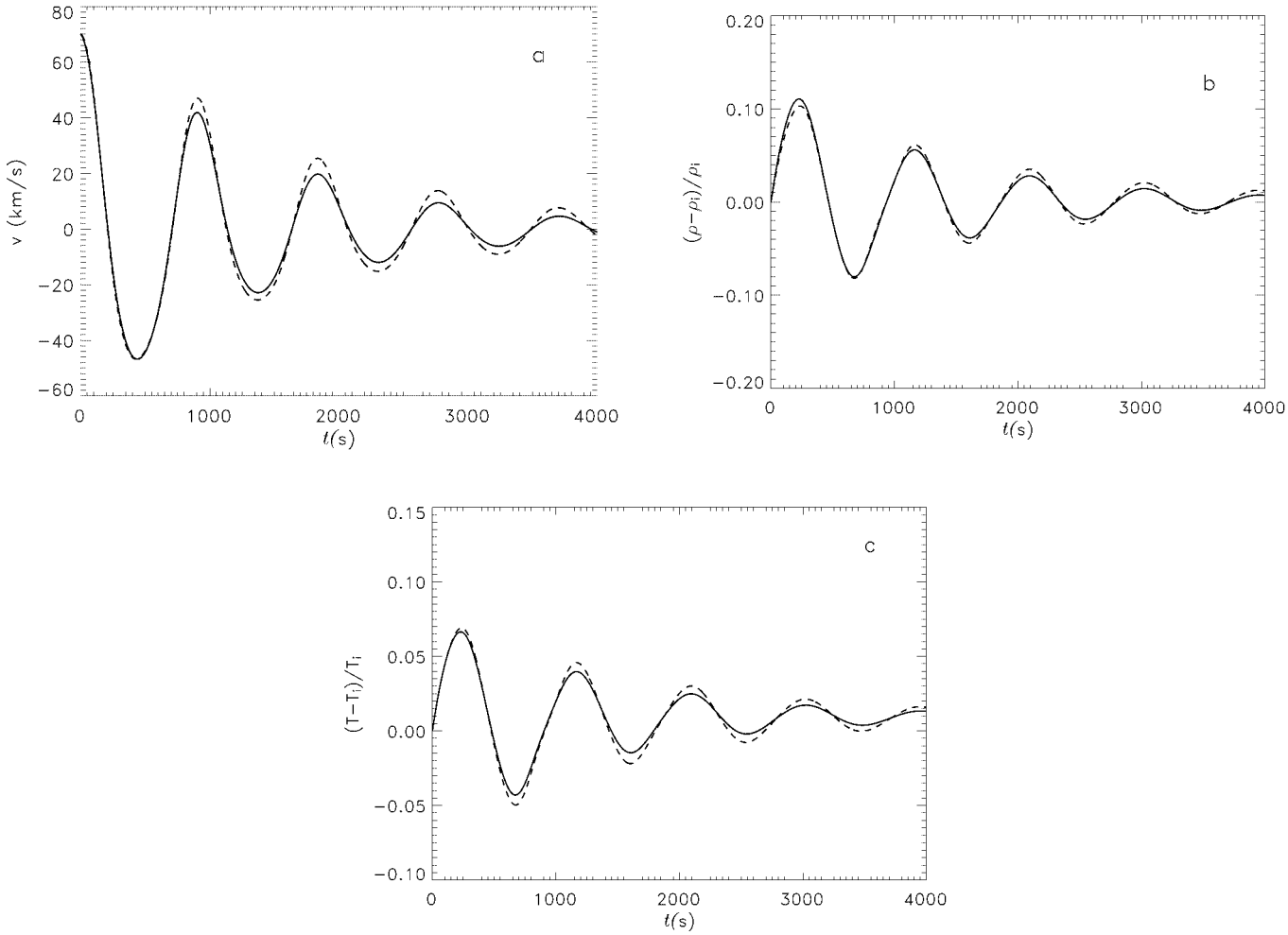

FIG. 4.—Time evolution of the (*a*) wave velocity, (*b*) density, and (*c*) temperature at $s = l_0 = 0.35L$ for the same model as in Fig. 2 but with no thermal conduction (i.e., $\kappa = 0$). In all panels, the time evolution of the waves in a stratified loop (*solid line*) is compared with that in a nonstratified medium (*dashed line*) for an initial wave-velocity amplitude of 84 km s^{-1}.

in shorter wave periods, with $P \approx 15.5$ and $\approx$15.6 minutes for the nonstratified and stratified ($T = 8.0$ MK) models, respectively. For comparison, the waves in the cooler ($T = 6.3$ MK) loop have periods of $\approx$17.2 minutes (nonstratified case) and $\approx$17.4 minutes (stratified case). From the values of τ_s quoted above, we can see that these periods are determined by the sound travel time, as expected in cases in which compressive viscosity is the dominant dissipation mechanism. In the nonstratified loops, the decay times are factors from $\sim$8 ($T = 6.3$ MK) to $\sim$2 ($T = 8.0$ MK) times longer than the ones obtained when both thermal conduction and compressive viscosity are allowed (see § 3.1), in agreement with previous findings by Ofman & Wang (2002). When stratification is accounted for, these factors decrease to $\sim$4 ($T = 6.3$ MK) and $\sim$1.4 ($T = 8.0$ MK), respectively, implying increased dissipation under the effects of gravity. This is a consequence of the larger velocity gradients achieved in the presence of stratification, which then lead to enhanced viscous dissipation.

On the other hand, when $\epsilon = 0$ (i.e., no viscosity) the linearized equations of De Moortel & Hood (2003) can be combined into the wave equations

$$\gamma \frac{\partial^2 T}{\partial t^2} = (\gamma - 1) \frac{\partial^2 p}{\partial s^2} + \gamma^2 d \frac{\partial}{\partial t} \left(\frac{\partial^2 T}{\partial s^2} \right), \tag{19}$$

$$\gamma \frac{\partial^2 v}{\partial t^2} = \frac{\partial^2 v}{\partial s^2} - \frac{\partial}{\partial t} \left(\frac{\partial T}{\partial s} \right), \tag{20}$$

$$\gamma \frac{\partial^2 \rho}{\partial t^2} = \frac{\partial^2 \rho}{\partial s^2} + \frac{\partial^2 T}{\partial s^2} \tag{21}$$

for the time evolution of the temperature, velocity, and density oscillations. Now we can see that dissipation by thermal conduction affects primarily the temperature, while the velocity and density waves are dissipated through hydrodynamic coupling with the temperature gradients. In Figure 5 we display the time evolution of all three waves in the absence of viscosity ($\eta = 0$) for $T = 8.0$ MK and $v_0 = 87$ km s^{-1}. As in Figures 2 and 4, the solid and dashed lines describe, respectively, the evolution in the presence and absence of stratification. As the thermal ratio increases from $d \approx 0.23$ (for $T = 6.3$ MK) to ≈ 0.36 (see Fig. 5 for $T = 8.0$ MK), the amplitudes of the temperature wave lower by a factor of $\sim$2 during the first period, while those of the density and velocity waves are not significantly affected. Further evolution proceeds, with the temperature wave being more strongly dissipated when $T = 8.0$ MK (Fig. 5*c*). However, the converse occurs for the velocity (Fig. 5*a*) and density (Fig. 5*b*) oscillations, which exhibit stronger damping of their amplitudes when $T = 6.3$ MK. This happens essentially because larger gradients of

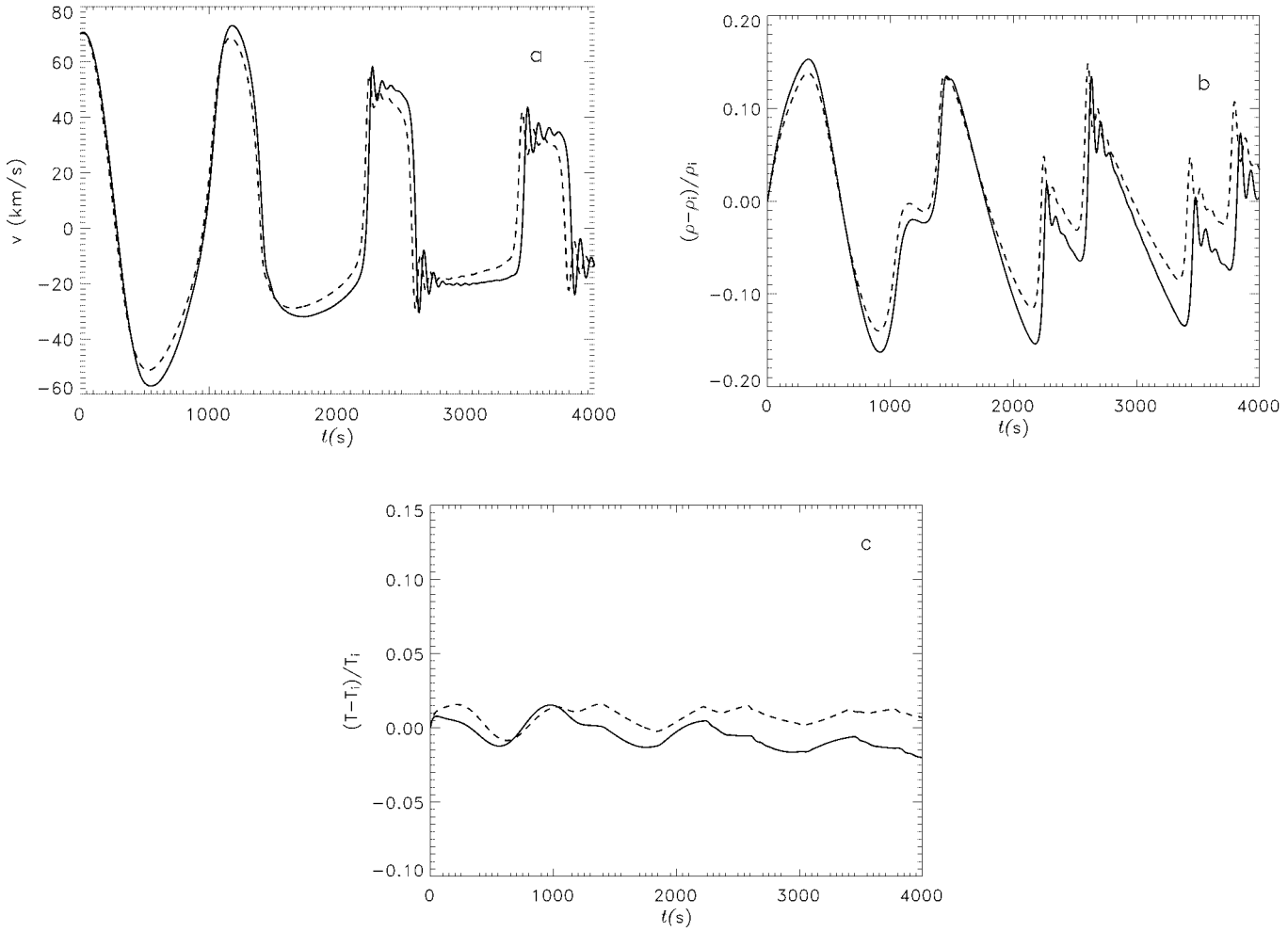

FIG. 5.—Time evolution of the (*a*) wave velocity, (*b*) density, and (*c*) temperature at $s = l_0 = 0.35L$ for the same model as in Fig. 2 but with no viscosity (i.e., $\eta = 0$). In all panels, the time evolution of the waves in a stratified loop (*solid line*) is compared with that in a nonstratified medium (*dashed line*) for an initial wave-velocity amplitude of 84 km s^{-1}.

T are generated at higher temperatures, which then contribute to increased dissipation of the thermal wave at $T = 8.0$ MK. However, the temporal and spatial variations of these gradients are smaller in the hotter loops compared to the cooler ones, thereby causing less dissipation of the density and velocity waves at higher temperatures. A straightforward comparison of Figures 4 and 5 clearly shows that density and velocity waves are more strongly dissipated by compressive viscosity, while temperature waves are mostly damped by thermal conduction. In addition, note that the suppression of viscosity allows for increased nonlinearity, as evidenced by the presence of high-order harmonics in the waves of Figure 5. In the nonstratified loops, the periods and decay times are, respectively, ≈21.3 and ≈97.6 minutes for $T = 6.3$ MK, and ≈19.4 and ≈100.6 minutes for $T = 8.0$ MK. For comparison, the waves in the stratified loops have periods of ≈21.8 ($T = 6.3$ MK) and ≈19.7 minutes ($T = 8.0$ MK) and have much longer decay times (≈189.7 minutes for $T = 6.3$ MK and ≈141.3 minutes for $T = 8.0$ MK). Thus, the decay times due to thermal conduction alone are factors of ∼3–7 times longer than the observed ones. In addition, the wave amplitudes are larger in the stratified cases, as opposed to when only viscous dissipation is allowed (Fig. 4). This occurs because of the larger velocity gradients induced by gravity, which in the absence of compressive viscosity contributes to wave amplification. This simple analysis shows that the concurrence of both thermal conduction and compressive viscosity is necessary in order to match the observations.

3.3. *Dependence of the Decay Time on Physical Loop Parameters*

We now study the variation of the decay time of standing slow-mode waves with temperature, total loop length, and wave-velocity amplitude in stratified hot loop models. In particular, the damping time as a function of the temperature is shown in Figure 6 for $v_0 = 20$ (*dashed line*) and 87 km s^{-1} (*solid line*), as obtained for two separate sequences of model calculations with fixed loop length (400 Mm) and temperatures varying from $T = 6.3$ to 8.0 MK. We see that the decay time always decreases with temperature in hot loops because of the increasing dissipative effects of thermal conduction and compressive viscosity at such high temperatures. For $v_0 = 87$ km s^{-1}, the wave amplitude at $s = l_0 = 0.35L$ is ≈$0.10L$, while for $v_0 = 20$ km s^{-1} it is only ≈$0.02L$, implying that, for a given temperature, standing waves of lower amplitudes decay in a shorter time. In particular when $T = 6.3$ MK, the damping time for $v_0 = 87$ km s^{-1} is about 300 s longer than when $v_0 = 20$ km s^{-1}. However, this difference reduces to about 60 s when the loop temperature is increased to $T = 8.0$ MK. Since the pressure scale height at $s = l_0$ is much larger (≈$1.75L$ for

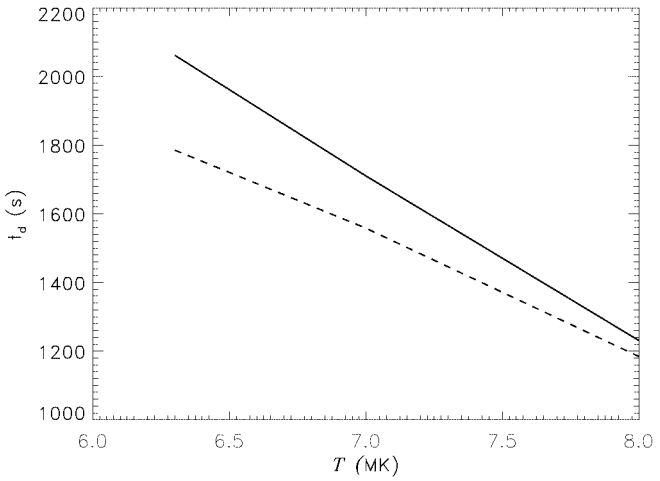

FIG. 6.—Dependence of the decay time t_d on loop temperature T, as obtained from two independent sequences of calculations with fixed loop length (400 Mm) and temperatures varying from $T = 6.3$ to 8.0 MK. The solid and dashed lines correspond to $v_0 = 87$ and 20 km s^{-1}, respectively.

$T = 6.3$ MK and $\approx 2.23L$ for $T = 8.0$ MK) than the wave amplitudes, we expect nonlinear effects to be rather small. This explains the almost linear decrease of the decay time with temperature for $v_0 = 87$ km s^{-1} (*solid line*), which obeys the approximate scaling $t_d \propto T^{-2.16}$. For the lower amplitude case ($v_0 = 20$ km s^{-1}; *dashed line*), the linear scaling makes a transition from $t_d \propto T^{-1.29}$ (slower decrease) at lower temperatures to $t_d \propto T^{-2.05}$ (more rapid decrease) at higher temperatures. This change of slope at ≈ 7.0 MK is a signature of the increasing dissipative effects of thermal conduction and viscosity at higher temperatures. We may then expect that in hotter loops ($T \gtrsim 8.0$ MK), slow MHD waves of differing amplitudes may dissipate on roughly the same timescale.

The dependence of the decay time on loop length is plotted in Figure 7 for four separate sequences of model calculations with varying length from 100 to 400 Mm and fixed temperature and wave-velocity amplitude. In general, as the loop length is increased, the decay time of slow magnetosonic waves also increases. This result is consistent with dissipation by thermal conduction and viscosity being more efficient in the shortest loops. The increase of the decay time with length is seen to occur at a comparatively faster rate when $T = 6.3$ MK and $v_0 = 87$ km s^{-1} (*dot-dashed line*). When $T = 8.0$ MK (*solid and dotted lines*), the decay time becomes fairly independent of the wave amplitude for all lengths considered. Note that for $T = 6.3$ MK, the same is true for loops with lengths $\lesssim 200$ Mm, which again confirms the previous finding that the size of the wave amplitude does not affect the decay time, provided that dissipation occurs efficiently. We also note that for all sequences, the increase of t_d with length becomes almost linear for $L \gtrsim 200$ Mm, in accordance with the relation $P \approx 2L/c_s$ (Roberts et al. 1984). This approximate linear dependence of the period on loop length has also been found to match the observed periods rather well (Wang et al. 2003a, 2003b). In particular, the linear behavior is found to obey the approximate scalings $t_d \propto L^{1.76}$ (for $T = 8.0$ MK and $v_0 = 87$ km s^{-1}), $t_d \propto L^{1.70}$ (for $T = 8.0$ MK and $v_0 = 20$ km s^{-1}), $t_d \propto L^{1.48}$ (for $T = 6.3$ MK and $v_0 = 87$ km s^{-1}), and $t_d \propto L^{1.35}$ (for $T = 6.3$ MK and $v_0 = 20$ km s^{-1}). The fact that, for a given length, the decay time of oscillations is shorter for the $T = 8.0$ MK loops is again indicative of dissipation operating more efficiently at higher temperatures. Moreover, the result that for all sequences, the shortest decay times occur in the smallest loops (of lengths 100–200 Mm) also argues in favor of thermal conduction and compressive viscosity as the primary mechanisms for slow-mode wave dissipation.

Finally, Figure 8 depicts the variation of the decay time with the initial wave-velocity amplitude v_0, as obtained from two independent sequences of model calculations with varying amplitudes from $v_0 = 20$ to 200 km s^{-1} and fixed temperature ($T = 6.3$ [*solid line*] and 8.0 MK [*dotted line*]) and loop length ($L = 400$ Mm). For both sequences, the decay time first increases with increasing initial wave amplitude until a maximum is reached around $v_0 \approx 120$ km s^{-1} for $T = 6.3$ MK and ≈ 100 km s^{-1} for the $T = 8.0$ MK sequence. For initial wave-velocity amplitudes higher than these values, the damping time is seen to decrease. The presence of a maximum in both sequences may be due to nonlinear effects. In fact, after the first period of oscillation, the wave amplitudes at the observation

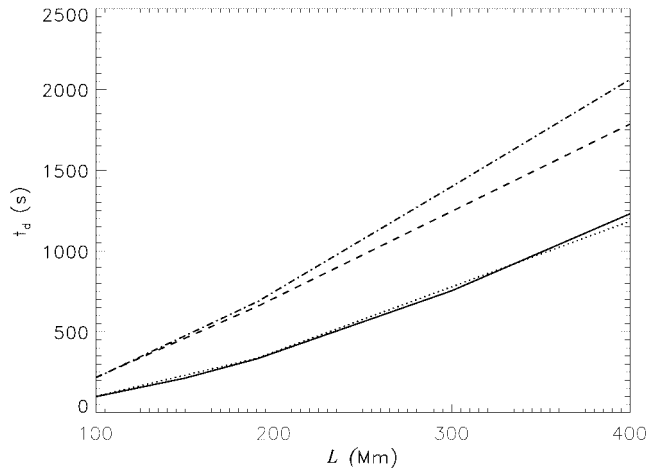

FIG. 7.—Dependence of the decay time t_d on loop length L, as obtained from four independent sequences of calculations having a fixed temperature ($T = 6.3$ or 8.0 MK), fixed initial wave-velocity amplitude ($v_0 = 20$ or 87 km s^{-1}), and loop lengths varying from $L = 100$ to 400 Mm. The solid ($v_0 = 87$ km s^{-1}) and dotted ($v_0 = 20$ km s^{-1}) curves correspond to model sequences with $T = 8.0$ MK, while the dashed ($v_0 = 20$ km s^{-1}) and dot-dashed ($v_0 = 87$ km s^{-1}) curves correspond to sequences with $T = 6.3$ MK.

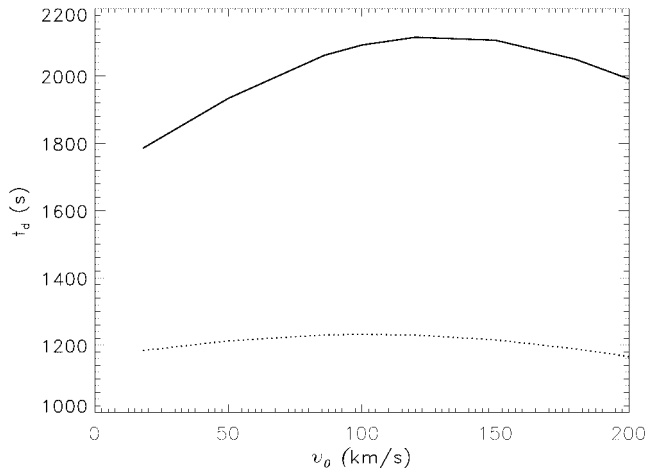

FIG. 8.—Dependence of the decay time t_d on the initial wave-velocity amplitude v_0, as obtained for two separate sequences of calculations with fixed loop temperature and length (400 Mm). Models with initial wave amplitudes between 20 and 200 km s^{-1} are considered. The solid and dotted curves correspond to $T = 6.3$ and 8.0 MK, respectively.

point $s = l_0 = 0.35L$ become $\gtrsim 0.10L$ when $v_0 \geq 100$ km s^{-1} in the $T = 8.0$ MK sequence and $\gtrsim 0.17L$ when $v_0 \geq 120$ km s^{-1} in the $T = 6.3$ MK loops, implying that nonlinear effects come out as the wave amplitude becomes a nonnegligible fraction of the pressure scale height. It is evident from Figure 8 that the predicted decay times are in the range 29–35 minutes for $T = 6.3$ MK and 19–21 minutes for $T = 8.0$ MK. These values are all within the inferred range of exponential decay times (5.7–36.8 minutes) of detected Doppler-shift oscillations observed with SUMER. We see from Figure 7 that a better spread of the decay times, covering the full observational data set, can be obtained by decreasing the total loop length in the model calculation sequences of Figure 8.

4. CONCLUSIONS

We have performed exploratory hydrodynamic calculations of the damping of slow magnetosonic waves in hot ($T >$ 6.0 MK) coronal loops, starting with loop parameters motivated by SUMER and *Yohkoh* SXT observations and including the effects of solar gravity, self-consistent heating, and large dissipation by heat conduction and compressive viscosity. In contrast to previous use of the model by Ofman & Wang (2002), here we investigate the effects of stratification on wave damping in hot coronal loops.

We find that stratification contributes a $\sim$10%–20% reduction of the decay time of slow MHD waves compared to the nonstratified loop models. In contrast to previous analyses and calculations, we also find that density and velocity oscillations are more efficiently dissipated by compressive viscosity, while temperature fluctuations are more strongly damped by thermal conduction. However, the concurrence of both mechanisms is necessary to match the observed periods and decay times of Doppler-shift oscillations. The predicted decay times are always determined by the thermal conduction timescale. Higher dissipation rates are observed in stratified loops as a result of the larger velocity gradients induced by gravity, which in turn lead to enhanced viscous dissipation. The predicted periods and decay times are all within the range of values inferred for the Doppler-shift oscillations observed by SUMER in hot coronal loops. For the range of temperatures (6–10 MK) characterizing hot coronal loops, the decay time of oscillations decreases linearly with temperature in stratified loops, with the rate of decrease being more sensitive to the size of the oscillation amplitudes at lower temperatures. In hot ($T >$ 7.0 MK) loops, the decay time becomes almost independent of the size of the wave amplitude, because of the overwhelming dissipative effects of thermal conduction and compressive viscosity at high temperatures. The results also indicate that the decay time of oscillations increases almost linearly with the loop length, in agreement with recent observations. In particular, the longest wave-damping times are obtained for the case of relatively high initial wave-velocity amplitudes ($v_0 \lesssim$ 120 km s^{-1}) in loops with $T = 6.3$ MK. In hotter ($T =$ 8.0 MK) loops, the decay time shortens, and its linear variation with loop length becomes almost independent of the size of the oscillation amplitude. This latter result is also indicative of the increased effects of thermal conduction and compressive viscosity on wave dissipation at such high temperatures.

The present model calculations apply to damping of slow MHD waves in one-dimensional loops of semicircular shape and constant cross-sectional area. In these simplified models, we have neglected the coupling of the loop with the chromosphere and the radiative losses. However, in a first approximation, for the long-period oscillations observed by SUMER, these effects may be of secondary importance, so we expect that our results will not be considerably affected by these assumptions. On the other hand, the effects of radiative losses may become important in loop configurations starting with nonuniform temperature profiles. Further work in this direction will focus on studying the damping of slow-mode waves in stratified hot loop models in which the temperature distribution is nonuniform.

We thank the anonymous referee for having provided a number of interesting and useful comments. His suggestions have contributed toward improving both the presentation of the results and the style of the paper. C. A. M.-B. would like to thank the CDCHT of the Universidad de los Andes for financial support. R. E. acknowledges M. Kéray for patient encouragement and is grateful to NSF, Hungary (OTKA, grant T043741). C. A. M.-B. and L. G. S. thank the Fondo Nacional de Ciencia, Tecnología e Innovación (Fonacit) of Venezuela for partial support. This paper is financially supported by the Instituto Venezolano de Investigaciones Científicas.

REFERENCES

Aschwanden, M. J., De Pontieu, B., Schrijver, C. J., & Title, A. 2002, Sol. Phys., 206, 99
Aschwanden, M. J., Fletcher, L., Schrijver, C. J., & Alexander, D. 1999, ApJ, 520, 880
Aschwanden, M. J., Schrijver, C. J., & Alexander, D. 2001, ApJ, 550, 1036
Berghmans, D., & Clette, F. 1999, Sol. Phys., 186, 207
Braginskii, S. I. 1965, Rev. Plasma Phys., 1, 205
Chae, J., Poland, A. I., & Aschwanden, M. J. 2002, ApJ, 581, 726
DeForest, C. E., & Gurman, J. B. 1998, ApJ, 501, L217
De Moortel, I., & Hood, A. W. 2003, A&A, 408, 755
De Moortel, I., Hood, A. W., Ireland, J., & Walsh, R. W. 2002, Sol. Phys., 209, 89
De Moortel, I., Ireland, J., & Walsh, R. W. 2000, A&A, 355, L23
Domingo, V., Fleck, B., & Poland, A. I. 1995, Sol. Phys., 162, 1
Handy, B. N., et al. 1999, Sol. Phys., 187, 229
Kliem, B., Dammasch, I. E., Curdt, W., & Wilhelm, K. 2002, ApJ, 568, L61
Nakariakov, V. M., & Ofman, L. 2001, A&A, 372, L53
Nakariakov, V. M., Ofman, L., DeLuca, E., Roberts, B., & Davila, J. M. 1999, Science, 285, 862
Nakariakov, V. M., Verwichte, E., Berghmans, D., & Robbrecht, E. 2000, A&A, 362, 1151
Ofman, L., Nakariakov, V. M., & Sehgal, N. 2000, ApJ, 533, 1071
Ofman, L., Romoli, M., Poletto, G., Noci, G., & Kohl, J. L. 1997, ApJ, 491, L111
Ofman, L., & Wang, T. 2002, ApJ, 580, L85
Roberts, B., Edwin, P. M., & Benz, A. O. 1984, ApJ, 279, 857
Sakurai, T., Ichimoto, K., Raju, K. P., & Singh, J. 2002, Sol. Phys., 209, 265
Schrijver, C. J., Aschwanden, M. J., & Title, A. M. 2002, Sol. Phys., 206, 69
Sigalotti, L. Di G., & Mendoza-Briceño, C. A. 2003, A&A, 397, 1083
Wang, T. J., Solanki, S. K., Curdt, W., Innes, D. E., & Dammasch, I. E. 2002a, ApJ, 574, L101
———. 2002b, in Proc. 11th *SOHO* Workshop, From Solar Minimum to Maximum, ed. A. Wilson (ESA SP-508; Noordwijk: ESA), 465
———. 2002c, in Proc. IAU Colloq. 188, Magnetic Coupling of the Solar Atmosphere, ed. H. Sawaya-Lacoste (ESA SP-505; Noordwijk: ESA), 199
Wang, T. J., Solanki, S. K., Curdt, W., Innes, D. E., Dammasch, I. E., & Kliem, B. 2003a, A&A, 406, 1105
Wang, T. J., Solanki, S. K., Innes, D. E., Curdt, W., & Marsch, E. 2003b, A&A, 402, L17